Nanoscale

ARTICLE

Atomic-scale sliding friction on contaminated surface

Wengen Ouyang,[a,b] Astrid S. de Wijn,[c,d] and Michael Urbakh*[a,b]

Using non-equilibrium molecular dynamic simulations, we investigate the effect of adsorbates on nanoscopic friction measured in friction force microscopy (FFM) experiments. We find that the interplay between different channels of energy dissipation at the frictional interface may lead to non-monotonic dependence of the friction force on the adsorbate surface coverage and to strongly nonlinear variation of friction with normal load (non-Amontons' behavior). Our simulations suggest that the key parameter controlling the variation of friction force with the normal load, surface coverage and temperature is the time-averaged number of adsorbates confined between the tip and the substrate. Three different regimes of temperature dependence of friction in the presence of adsorbates are predicted. Our findings point on new ways to control friction on contaminated surfaces.

1. Introduction

Any surface that is exposed to ambient air will be contaminated by adsorbed molecules, such as hydrocarbons, oxygen, water or other small molecules.[1-4] The strength of adsorbate-substrate interaction and mobility of adsorbed molecules may change in a broad range depending on the mechanism of adsorption, which varies from weak physisorption to strong chemisorption. The adsorption of molecules on solid surfaces plays a key role in adhesion, friction and wear behaviours.[1, 4-9] Functioning of micro- and nano-devices involving mechanical motions is also strongly influenced by the presence of adsorbates,[10, 11] which may lead to severe friction and wear, and thus considerably reduce their durability. In particular, it has been found that adsorbed molecules can arrange to lock two contacting surfaces together resulting in the appearance of static friction even between incommensurate surfaces and in enhancement of kinetic friction.[1, 12, 13] Interestingly, molecular dynamics (MD) simulations demonstrated that in the case of molecules weakly adsorbed between two flat crystalline surfaces both static friction and kinetic friction forces only slightly depend on the adsorbate coverage.[1, 12, 14] In contrast, a strong dependence of friction on coverage has been predicted in MD simulations mimicking quartz crystal microbalance measurements, where adsorbed molecules slide on a crystalline surface.[15, 16] Recent experimental studies and simulations of sliding of rare-gas absorbed islands on metal surfaces demonstrated a significant contribution of island edges to friction forces and found a

transition from superlubric adsorbate motion to the pinned state when the coverage approaches a full monolayer.[6, 15-17] Furthermore, phase changes in strongly confined molecular layers can produce nontrivial effects on lubrication.[18]

Up to now, the vast majority of experimental studies of nanoscale friction have been performed using friction force microscopy (FFM). However, the modelling work has generally relied on MD simulations in which adsorbed molecules are confined between opposing flat plates in relative motion or slide on a surface.[1, 12-22] Such simulations don't reflect the geometry of FFM experiments, and as a result they don't correctly represent the shear induced motion of adsorbed molecules and frictional dissipation. Therefore, a major goal of our work is to address these problems and to understand mechanisms of frictional dissipation in FFM measurements at contaminated surfaces.

In this Letter, we use non-equilibrium MD simulations to investigate the effect of adsorbates on nanoscopic friction measured in FFM experiments. We demonstrate that the interplay between different channels of energy dissipation at the frictional interfaces may lead to non-monotonic dependence of the friction force on the adsorbate surface coverage. We establish conditions, under which strongly nonlinear variation of friction with normal load (non-Amontons' behaviour) should be observed and predict three different regimes of temperature dependence of friction in the presence of adsorbates.
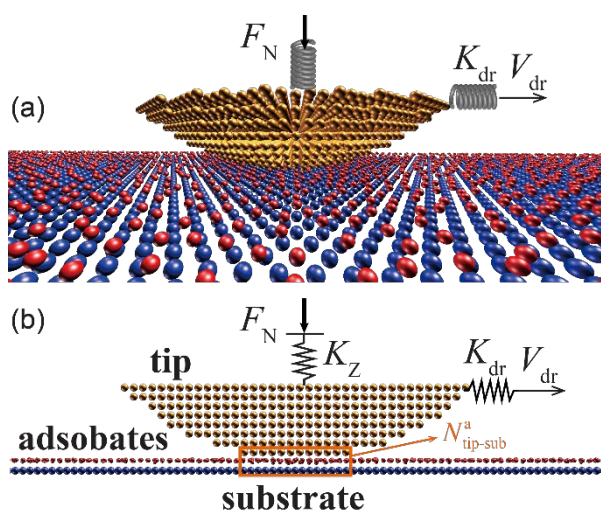
2. Model

Our simulation setup, aims to mimic FFM experiments under ambient conditions, where surfaces are covered by adsorbates. It is schematically presented in Fig. 1. The tip is represented by crystalline spherical cap, whose center of mass is coupled to the FFM stage by springs $K_X = K_Y = K_\parallel$ in the lateral x, y directions. The stage moves with a constant velocity, V_{dr},

a. School of Chemistry, Tel Aviv University, Tel Aviv 69978, Israel. Email: urbakh@post.tau.ac.il
b. The Sackler Center for Computational Molecular and Materials Science, Tel Aviv University, Tel Aviv 6997801, Israel
c. Department of Mechanical and Industrial Engineering, Norwegian University of Science and Technology, 7491 Trondheim, Norway
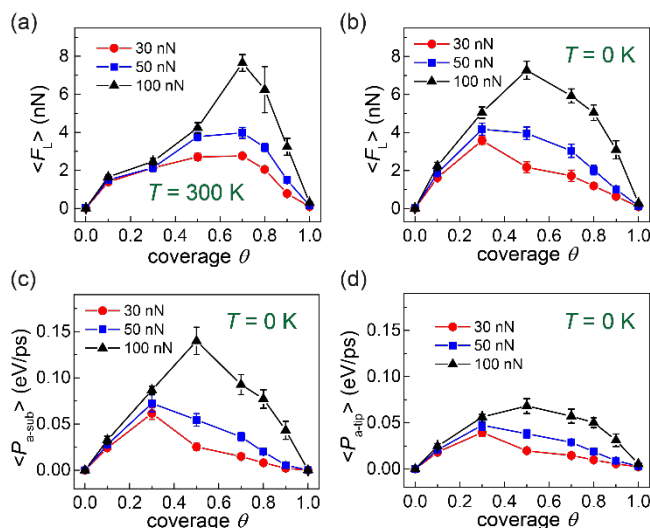d. Department of Physics, Stockholm University, 10691 Stockholm, Sweden

Fig. 1 (a) The schematic sketch of the model geometry. (b)The adsorbates located in the orange rectangular region are referred as confined adsorbed molecules.

Fig. 2 Friction force ($\langle F_L \rangle$) as a function of coverage calculated for different normal loads and temperatures of $T = 300$ K (a) and $T = 0$ K (b). (c-d) The rates of energy dissipation to the substrate $P_{a\text{-sub}}$ and to the tip $P_{a\text{-tip}}$, respectively. Here, $U_0 = 0.38$ eV, $r_e = 2.65$ Å, $\alpha = 1.47$ Å^{-1}, $\varepsilon_{a\text{-tip}} = 30$ meV, $\sigma_{a\text{-tip}} = 3$ Å, $\varepsilon_{tip\text{-sub}} = 50$ meV, $\sigma_{tip\text{-sub}} = 2.7$ Å, $\varepsilon_{a\text{-a}} = 2.757$ meV, $\sigma_{a\text{-a}} = 3.4$ Å.

along the surface in x-direction. A normal load is applied to the tip in the direction perpendicular to the substrate (z direction) through the spring with stiffness K_Z, which is connected to the stage fixed in z-direction. Our quantity of interest is the kinetic friction force, $\langle F_L \rangle$, defined as the time-averaged external spring force acting on the tip in the pulling direction.

The frictional dissipation is determined by the shear induced dynamics of the adsorbed layer, which depends on the interactions of adsorbate with the substrate and the tip and on the interactions within the layer. We describe the interactions between the adsorbates and substrate atoms using a Morse potential with the strength, U_0, between 0.1 and 5 eV. This range allows us to investigate different regimes of adsorption, from weak physisorption to strong chemisorption. The adsorbate-tip and adsorbate-adsorbate interactions are modelled by Lennard-Jones (LJ) potentials with the depths of the potential wells $\varepsilon_{a\text{-t}} = 5\text{-}120$ meV and $\varepsilon_{a\text{-a}} = 2.757$ meV, respectively. These values lie in the range of typical energies for the interactions between common adsorbates and between the adsorbates and substrates.[1, 23-28] In the simulations both the substrate and the tip are considered as rigid FCC crystals with the (111) R0° and (110) R0°, surfaces in the horizontal plane and lattice spacings of 0.288 nm and 0.361 nm, respectively. Hence, mimicking a gold substrate and copper tip. The radius of the tip is chosen to be 5 nm. The simulations are performed in LAMMPS[29] and the temperature is controlled by a Langevin thermostat (see Methods for details).

3. Non-monotonic dependence of the friction force on the adsorbate surface coverage

Figs. 2(a) and (b) report the kinetic friction force, $\langle F_L \rangle$, as a function of the adsorbate surface coverage, θ, calculated for temperatures of 300 K and 0 K, respectively, and for a number of different normal loads. For both temperatures the friction

force exhibits a non-monotonic dependence on θ with maxima lying at moderate coverages. The lowest values of $\langle F_L \rangle$ are achieved in the absence of adsorbates and for full surface coverage. The observed non-monotonic variation of the friction force with θ results from the dependence of shear-induced dynamics in the adsorbed layer on the adsorbate coverage. For low and moderate coverages the tip drags the adsorbates along the surface, whereas for higher coverages the tip slides above the adsorbates, which are stuck at the surface oscillating near their equilibrium positions. The low friction forces found for $\theta \sim 0$ and $\theta \sim 1$ (see Figs. 2(a) and (b)) are explained by the incommensurability of the substrate surface and the adsorbed layer lattices with respect to the tip surface lattice. The results presented in Fig. 2 were obtained for the strength of the adsorbate-substrate interaction $U_0 = 0.38$ eV. However, a similar variation of $\langle F_L \rangle$ with θ was found in the entire range of studied parameters.

To get a quantitative insight into the physical origin of the intriguing non-monotonic variation of the friction force with θ, we have examined the coverage dependence of the time-averaged rate of energy dissipation during the sliding motion. The latter can be written as a sum of contributions of different dissipation channels, $P_{tot} = P_{a\text{-sub}} + P_{a\text{-tip}} + P_{tip}$, where $P_{a\text{-sub}}$ and $P_{a\text{-tip}}$ are the rates of energy dissipated by the adsorbates into the substrate and into the tip, respectively, and P_{tip} describes the rate of dissipation of the tip kinetic energy directly to the substrate and surrounding medium. In our simulations, the last term is considerably (more than five times) smaller than the first two terms. The explicit equations for $P_{a\text{-sub}}$, $P_{a\text{-tip}}$ and P_{tip} are presented in the Methods Section.

In order to isolate the shear-induced dissipation from thermal effects, we present in Fig. 2(c) and d the rates of energy dissipation, $P_{a\text{-sub}}$ and $P_{a\text{-tip}}$ as functions of the adsorbate coverage, calculated at zero temperature. Both rates increase
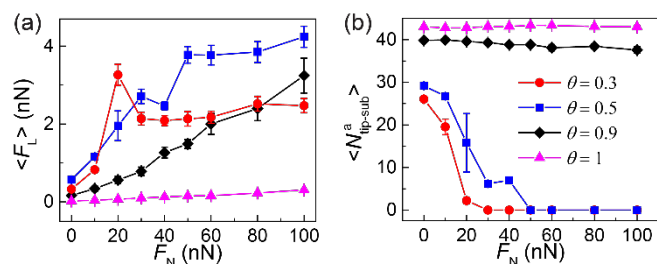
Fig. 3 The friction force ($\langle F_L \rangle$) (a) and the time-averaged number of adsorbates confined between the tip and the substrate, $\langle N_{tip-sub}^a \rangle$. (b) as functions of normal load (F_N) calculated for four different coverages ($\theta = 0.3, 0.5, 0.9, 1$). See Fig. 1(b) for the definition of $\langle N_{tip-sub}^a \rangle$. Here $U_0 = 0.38$ eV and $T = 300$ K. Other parameters are the same as that in Fig. 2.

with θ at low coverages, show maxima at moderate coverages, and decrease with further increase in θ. This behaviour can be understood by noting that the rates P_{a-sub} and P_{a-tip} are proportional to the number of adsorbates located in close proximity to the tip and their squared velocities relative to the substrate and tip, respectively. The first factor grows with θ up to $\theta \sim 0.5$ and then approximately levels off. The adsorbate velocities, induced by the interaction with the sliding tip decrease with increasing θ, since the adsorbate-adsorbate repulsion prevents the adsorbate motion. In addition, the mismatch between the lattices of the tip and of the adsorbate layer results in significant reduction of the rate of energy dissipation into the tip for $\theta \sim 1$. The interplay between these effects leads to the non-monotonic dependence of P_{a-sub} and P_{a-tip} on θ, which can be seen in Fig. 2(c)-(d). Since the friction force is proportional to the rate of energy dissipation,[30] this explains the non-monotonic dependence on the adsorbates surface coverage.

4. Non-Amontons' frictional behaviour

The dependence of the kinetic friction force on the normal load, F_N, which is one of the main tribological characteristics, is presented in Fig. 3(a). We found that for high surface coverages, $\theta \geqslant 0.8$, the friction force grows approximately linearly with increasing normal load, exhibiting the Amonton's law, whereas for lower coverages our simulations predict a highly nonlinear variation of $\langle F_L \rangle$ with F_N. The results of simulations performed for $\theta = 0.3$ and $\theta = 0.5$ exhibit two distinct regimes of friction characterized by considerably different friction coefficients, which were extracted from the slope of the friction forces as a function of the normal load. In the first regime observed for low normal loads ($F_N < 20$ nN for $\theta = 0.3$ and $F_N < 30$ nN for $\theta = 0.5$) we found the friction coefficients of 0.07 and 0.14 for $\theta = 0.3$ and $\theta = 0.5$, respectively. In the second regime occurring for high loads ($F_N > 30$ nN for $\theta = 0.3$ and $F_N > 50$ nN for $\theta = 0.5$) the friction coefficients drop by approximately an order of magnitude to 0.008 and 0.009 for $\theta = 0.3$ and $\theta = 0.5$, respectively. In the interval of normal loads corresponding to the transition regions, a maximum in the friction force as a function of normal load can appear, resulting in a negative friction coefficient. With increasing of strength of adsorbate-

substrate interaction, the transition between the described regimes of friction shifts to higher values of normal load.

Our simulations suggest that the key parameter controlling the dependencies of friction on normal load, temperature and strength of adsorbate-substrate interaction is the time-averaged number of adsorbates confined between the tip and the substrate (see Fig. 3-5). Here, the adsorbates located below the circular area of radius of ~1 nm centered at the tip apex were considered to be confined adsorbates. Fig. 3(b) shows that for $\theta \leqslant 0.8$ and low normal loads (the first friction regime), a number of confined adsorbates decreases sharply with increasing F_N, and correspondingly the normal load per adsorbate increases significantly. As a result, the frictional dissipation at the adsorbate-tip and adsorbate-substrate interfaces increases considerably with F_N, leading to a relatively high friction coefficient. For higher normal loads, the tip penetrates into the adsorbed layer and adsorbates are squeezed out from the confined region. In this second regime, the main contribution to the frictional energy dissipation comes from the adsorbates pushed by the tip along the surface. This contribution depends weakly on the normal load, leading to a low friction coefficient. The mechanism of load dependence of friction is different for high surface coverages ($\theta \geqslant 0.8$), where the number of adsorbates confined between the tip and the surface only slightly decreases with increasing normal load, and the friction force increases almost linearly with F_N (see Fig. 3(a)). In this case, the tip slides above the adsorbed layer and the friction coefficient decreases with the increase of θ, since the mobility of the adsorbed molecules decreases, and the structure of adsorbed layer becomes incommensurate compared with that of the tip.

5. Effect of strength of adsorbate-substrate interaction on friction

The results discussed above have been obtained for the strength of the adsorbate-substrate interaction of 0.38 eV, which corresponds to a case of weak chemisorption. However, depending on the mechanism of adsorption (for instance, physisorption vs. chemisorption) the value of U_0 may vary in a wide range. Fig. 4(a) shows how the variation of U_0 influences the friction force.
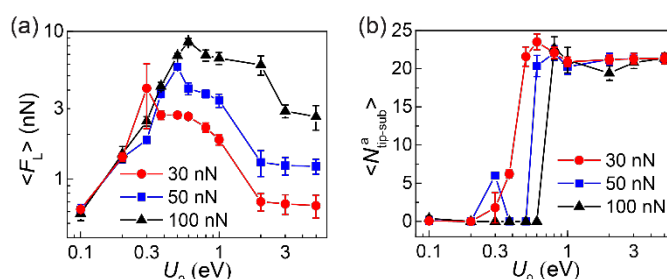
Fig. 4 (a) The friction force ($\langle F_L \rangle$) (a) and the average number of adsorbates located between the tip and the substrate ($\langle N_{tip-sub}^a \rangle$). (b) as functions of energy depth U_0 calculated for two different normal loads. Here, $\theta = 0.5$ and $T = 300$ K. Other parameters as in Fig. 2.

Here, we present results obtained for $\theta = 0.5$, F_N = 30, 50 and 100 nN and the interaction energy, U_0, changing from 0.1 to 5 eV. Interestingly, the friction force exhibits non-monotonic dependence on U_0 with a maximum lying in the range of 0.3-0.5 eV depending on the normal load. The physical origin of this dependence can be understood by considering the effect of U_0 on the number of adsorbates confined between the sliding tip and the substrate surface (see Fig. 4(b)).

Fig. 4(b) shows that in the range of U_0 and normal loads, where the adsorbates are squeezed out from the confined region, the friction increases with the strength of the adsorbate-substrate interaction. In this regime, the main contribution to the frictional energy dissipation is provided by the adsorbates pushed by the tip along the surface. The rate of dissipation of adsorbate kinetic energy into the substrate, and correspondingly the friction force, are proportional to the height of potential barriers opposing the adsorbate sliding on the substrate surface.[13, 31] In turn, the barrier heights are proportional to U_0, which explains the almost linear increase in $\langle F_L \rangle$ with U_0 before reaching the maximum (see Fig. 4(a)). Notably, for relatively low values of U_0 ($U_0 < 0.3$eV) the $\langle F_L \rangle$ vs. U_0 curves coincide for different loads, because the described above mechanism of energy dissipation rate is independent of the load.

For higher values of U_0 (0.3 eV $< U_0 < 2$ eV for $F_N = 30$ nN, and 0.6 eV $< U_0 < 3$ eV for $F_N = 100$ nN), the tip slides above the adsorbed layer, and the energy dissipation occurs at both adsorbate-tip and adsorbate surface interfaces. In this regime, the rates of energy dissipation into the tip and substrate are determined by the adsorbate velocities relative to the tip and the substrate, respectively. With increasing U_0, the adsorbate mobility is reduced and the adsorbate velocity decreases. This effect leads to the reduction of the friction force with U_0 shown in Fig. 4(a). For very large vales of U_0 ($U_0 > 2$ eV for $F_N = 30$ nN and $U_0 > 3$ eV for $F_N = 100$ nN,) the adsorbates are stuck to the substrate and do not slide over the surface, so that the energy dissipation occurs only at the adsorbate-tip interface, and the friction force as a function of U_0 levels off.

6. Temperature dependence of friction

Additional insight into microscopic mechanisms of friction at surfaces covered by adsorbates may be gained considering the temperature dependence of friction. Results of corresponding simulations performed for $\theta = 0.5$, $U_0 = 0.38$ eV are presented in Fig. 5(a), showing that the variation of friction with temperature may be highly dependent on the normal load, which controls regimes of friction. As mentioned above, we can understand this by considering the effect of temperature on the number of adsorbates confined between the tip and the substrate (see Fig. 5(b)).

The comparison of Fig. 5(a) and (b) shows that the friction force as a function of temperature exhibits the following features: (i) a gentle increase with increasing T when the number of adsorbates confined between the tip and the surface decreases (red circles). (ii) a decrease with T in the absence of confined adsorbates (black triangles). (iii) a considerable
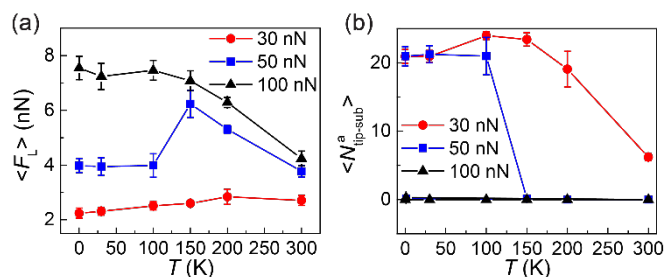

Fig. 5 The friction force ($\langle F_L \rangle$) (a) and the time-averaged number of adsorbates located between the tip and the substrate ($\langle N^a_{tip-sub} \rangle$). (b) as functions of temperature calculated for three normal loads. Here, $\theta = 0.5$ and $U_0 = 0.38$ eV. Other parameters as in Fig. 2.

enhancement of $\langle F_L \rangle$ at the transition between the above regimes. The first effect results from an increase in the normal load per confined adsorbate that leads to an increase of heights of sliding potential energy barriers at the adsorbate-tip and adsorbate-substrate interfaces. The increase of friction caused by this effect is partially compensated by the effect of thermal activation, which facilitates transitions over the barriers. The second regime of variation of friction with temperature is similar to that predicted by the Prandtl-Tomlinson model.[32] Here, the observed reduction of friction with temperature is due to the thermally activated motion by the adsorbates, which are pushed by the tip over the potential energy barriers at the substrate surface. The increase in the friction force in the transition between the two discussed regimes is due to the tip penetration into the adsorbed layer resulting in the increase of number of adsorbates pushed by the tip. This leads to the enhancement of the energy dissipation at the adsorbate-substrate interface, and to the increase of the overall friction force.

7. Conclusions

In summary, our MD simulations predict a non-monotonic dependence of the friction force on the adsorbate surface coverage and a strongly nonlinear variation of friction with normal load (non-Amontons' behaviour). These intriguing behaviours result from the interplay between different channels of energy dissipation involved in a frictional motion of FFM tip sliding at contaminated surfaces. Our simulations suggest that the key parameter controlling the variation of friction force with the normal load, adsorbate surface coverage and temperature is the time-averaged number of adsorbates confined between the tip and the substrate. We found two different regimes of fictional motion corresponding to the sliding of the tip above the adsorbed layer and the tip penetration in the layer are characterized by significantly different friction coefficients and exhibit drastically different temperature dependences of friction. In the interval of normal loads corresponding to the transitions between these regimes a maximum in the friction force as a function of the applied load can appear, resulting in a negative friction coefficient. For given external conditions, such as normal load, temperature and

adsorbate surface coverage, the observed regime of friction is determined by the strength of adsorbate-substrate interaction ranging from weak chemisorption to strong chemisorption. Revealing mechanisms of frictional energy dissipation suggests an avenue for controlling friction on contaminated surfaces by tuning the coverage of the adsorbed molecules.

8. Methods

The simulations were performed using LAMMPS.[29] The interaction between the substrate and adsorbates is described using the Morse potential,[15, 33] $U^{MP}(r)=U_0[e^{-2\alpha(r-r_e)}-2e^{-\alpha(r-r_e)}]$, where r is the distance between the adsorbed molecules and the substrate atoms, r_e is the equilibrium distance, U_0 is the energy well depth, and α controls the width of the potential. Typical values of parameters of the Morse potentials describing adsorbate-metal interactions lie in the range of[34]: $U_0 \sim 0.1$–1 eV, $r_e \sim 2.5$–6 Å and $\alpha \sim 0.5$–1.7 Å^{-1}. For instance, for Sulfur atoms absorbed on a gold surface [35] $U_0 = 0.38$ eV, $r_e = 2.65$ Å and $\alpha = 1.47$ Å^{-1}. The interactions between the tip and adsorbates, the tip and the substrate, and between the adsorbates have been described by Lennard-Jones (LJ) potential, $U_{LJ}(r)=4\varepsilon[(\sigma/r)^{12}-(\sigma/r)^6]$, where r is the distance between two atoms, σ is the equilibrium distance, ε is the energy well depth. Typical values of the interaction parameters ε and σ lie in the range of $\varepsilon \sim 1$-167 meV and $\sigma \sim 2$-5 Å.[1, 23-25, 27, 28, 36] The following values have been used in the simulations: (i) for the tip-adsorbate interactions $\varepsilon_{a\text{-tip}} = 30$ meV, $\sigma_{a\text{-tip}} = 3$ Å, (ii) for the tip-substrate interaction $\varepsilon_{tip\text{-sub}} = 50$ meV, $\sigma_{tip\text{-sub}} = 2.7$ Å and (iii) for the adsorbate-adsorbate interactions $\varepsilon_{a\text{-a}} = 2.757$ meV, $\sigma_{a\text{-a}} = 3.4$ Å.

The presented results have been obtained for the pulling velocity $V_{dr} = 5$ m/s, which is sufficiently low for the system to exhibit stick-slip behaviour. The stiffnesses of the external springs have been chosen as $K_X = K_Y = K_{dr} = 10$ N/m and $K_Z = 20$ N/m that are typical values used in the experiments. The mass and radius of the tip are 2.78×10^{-22} kg and 5 nm, respectively. In the simulations, we used the orthorhombic box with the size of 115.4 nm×11.243 nm×3 nm. Periodic boundary conditions have been applied in both x and y directions. The number of atoms in the tip is 2618 and the maximal number of the adsorbed particles corresponding to the full surface coverage by adsorbates is 38605. The friction force have been calculated as $\langle F_L \rangle = \langle K_{dr}(V_{dr}t - X_{tip})\rangle$, where $\langle \cdot \rangle$ denotes a steady-state time average. The statistical errors have been estimated using ten different sets of data, each over a time interval of 1.2 ns.

Unless otherwise stated, the simulations have been performed at room temperature (300 K). The temperature is controlled by a Langevin thermostat with damping coefficients $\eta^{sub}_{x,y,z}$ and $\eta^{tip}_{x,y,z}$, which account for the dissipation of kinetic energy of the adsorbate into the substrate and tip microscopic degrees of freedom. The damping coefficients decrease exponentially with the increase of distances between the adsorbate and the substrate or the center of sphere (COS) representing the tip, respectively,[37-39] as described by the following equations

$$\eta^{sub}_\alpha(z) = \eta^{sub}_{\alpha 0}\exp\left(1 - z/\sigma^{MP}_{sub}\right), \alpha = x,y,z, \tag{1}$$

$$\eta^{tip}_\alpha(|\boldsymbol{R}_t - \boldsymbol{r}_i|) = \eta^{tip}_{\alpha 0}\exp\left[1 - (|\boldsymbol{R}_t - \boldsymbol{r}_i| - R_{tip})/\sigma^{LJ}_{tip}\right], \tag{2}$$

where R_{tip} is the tip radius, $\boldsymbol{r}_i = (x_i, y_i, z_i)$ and $\boldsymbol{R}_t = (X, Y, Z)$ are the coordinates of the i-th adsorbate, and of the tip COS, respectively. $|\boldsymbol{R}_t - \boldsymbol{r}_i| = \sqrt{(x_i - X)^2 + (y_i - Y)^2 + (z_i - Z)^2}$, and $\eta^{sub}_{x0} = \eta^{sub}_{y0} = \eta^{sub}_{z0} = \eta^{tip}_{x0} = \eta^{tip}_{y0} = \eta^{tip}_{z0} = 1$ ps^{-1}. Thus, only adsorbates located in close proximity to the tip contribute significantly to the energy dissipation into the tip. In addition, to suppress vibration of the tip during sliding, we introduced the damping coefficients $\Gamma_{Y,Z}$, describing the dissipation of kinetic energy of the tip into the substrate and surrounding medium. For these parameters the critical values of the damping were chosen, $\Gamma_{Y,Z} = 2\sqrt{K_{Y,Z}M}$, where M is the mass of the tip.

The rates of energy dissipation into the substrate and the tip, P_{a-sub} and P_{a-tip}, can be written as

$$P_{a-\text{sub}} = m\left\langle\sum_{i=1}^{N}\left[\eta^{sub}_x(z_i)v^2_{i,x} + \eta^{sub}_y(z_i)v^2_{i,y} + \eta^{sub}_z(z_i)v^2_{i,z}\right]\right\rangle, \tag{3}$$

$$P_{a-\text{tip}} = m\left\langle\sum_{i=1}^{N}\left[\eta^{tip}_x(|\boldsymbol{R}_t - \boldsymbol{r}_i|)(v_{i,x} - V_X)^2 + \eta^{tip}_y(|\boldsymbol{R}_t - \boldsymbol{r}_i|)(v_{i,y} - V_Y)^2 + \eta^{tip}_z(|\boldsymbol{R}_t - \boldsymbol{r}_i|)(v_{i,z} - V_Z)^2\right]\right\rangle \tag{4}$$

$$P_{tip} = \Gamma_Y V^2_Y + \Gamma_Z V^2_Z \tag{5}$$

where m is the mass of an adsorbate, N is the total number of adsorbates, $\boldsymbol{v}_i = (v_{i,x}, v_{i,y}, v_{i,z})$ and $\boldsymbol{V}_t = (V_X, V_Y, V_Z)$ are velocities of the i-th adsorbate and of the tip COS, respectively.

Acknowledgements

References

1. G. He, M. H. Müser and M. O. Robbins, *Science*, 1999, **284**, 1650-1652.
2. Z. Li, A. Kozbial, N. Nioradze, D. Parobek, G. J. Shenoy, M. Salim, S. Amemiya, L. Li and H. Liu, *ACS Nano*, 2016, **10**, 349-359.
3. Z. Li, Y. Wang, A. Kozbial, G. Shenoy, F. Zhou, R. McGinley, P. Ireland, B. Morganstein, A. Kunkel, S. P. Surwade, L. Li and H. Liu, *Nat. Mater.*, 2013, **12**, 925-931.
4. S. H. Kim, D. B. Asay and M. T. Dugger, *Nano today*, 2007, **2**, 22-29.
5. C. C. Vu, S. Zhang, M. Urbakh, Q. Li, Q. C. He and Q. Zheng, *Phys. Rev. B*, 2016, **94**, 081405.
6. J. Krim, *Adv. Phys.*, 2012, **61**, 155-323.
7. M. Urbakh, J. Klafter, D. Gourdon and J. Israelachvili, *Nature*, 2004, **430**, 525-528.

8.   I. Szlufarska, M. Chandross and R. W. Carpick, *J. Phys. D: Appl. Phys.*, 2008, **41**, 123001.

9.   D. B. Asay, M. T. Dugger, J. A. Ohlhausen and S. H. Kim, *Langmuir*, 2008, **24**, 155-159.

10. D. B. Asay, E. Hsiao and S. H. Kim, *J. Appl. Phys.*, 2011, **110**, 064326.

11. A. J. Barthel, A. Al-Azizi, N. D. Surdyka and S. H. Kim, *Langmuir*, 2014, **30**, 2977-2992.

12. M. H. Müser and M. O. Robbins, *Phys. Rev. B*, 2000, **61**, 2335.

13. M. H. Müser, L. Wenning and M. O. Robbins, *Phys. Rev. Lett.*, 2001, **86**, 1295-1298.

14. M. D. Perry and J. A. Harrison, *J. Phys. Chem. B*, 1997, **101**, 1364-1373.

15. M. Pierno, L. Bruschi, G. Mistura, G. Paolicelli, A. di Bona, S. Valeri, R. Guerra, A. Vanossi and E. Tosatti, *Nat. Nanotechnol.*, 2015, **10**, 714-718.

16. N. Varini, A. Vanossi, R. Guerra, D. Mandelli, R. Capozza and E. Tosatti, *Nanoscale*, 2015, **7**, 2093-2101.

17. R. Guerra, E. Tosatti and A. Vanossi, *Nanoscale*, 2016, **8**, 11108-11113.

18. A. S. de Wijn and L. G. M. Pettersson, *Phys. Rev. B*, 2017, **95**, 165433.

19. J. N. Glosli and G. M. McClelland, *Phys. Rev. Lett.*, 1993, **70**, 1960-1963.

20. P. T. Mikulski and J. A. Harrison, *J. Am. Chem. Soc.*, 2001, **123**, 6873-6881.

21. M. Chandross, E. B. Webb, M. J. Stevens, G. S. Grest and S. H. Garofalini, *Phys. Rev. Lett.*, 2004, **93**, 166103.

22. C. D. Lorenz, M. Chandross, G. S. Grest, M. J. Stevens and E. B. Webb, *Langmuir*, 2005, **21**, 11744-11748.

23. S. J. Stuart, A. B. Tutein and J. A. Harrison, *J. Chem. Phys.*, 2000, **112**, 6472-6486.

24. A. K. Rappé, C. J. Casewit, K. Colwell, W. A. Goddard and W. Skiff, *J. Am. Chem. Soc*, 1992, **114**, 10024-10035.

25. Z.-Y. Ong and E. Pop, *Phys. Rev. B*, 2010, **81**, 155408.

26. S. Kawai, A. Benassi, E. Gnecco, H. Söde, R. Pawlak, X. Feng, K. Müllen, D. Passerone, C. A. Pignedoli and P. Ruffieux, *Science*, 2016, **351**, 957-961.

27. Z. Xu and M. J. Buehler, *ACS Nano*, 2009, **3**, 2767-2775.

28. P. Süle, M. Szendrő, G. Z. Magda, C. Hwang and L. Tapasztó, *Nano Lett.*, 2015, DOI: 10.1021/acs.nanolett.5b03886.

29. S. Plimpton, *J. Comput. Phys.*, 1995, **117**, 1-19.

30. B. N. J. Persson and A. Nitzan, *Surf. Sci.*, 1996, **367**, 261-275.

31. E. D. Smith, M. O. Robbins and M. Cieplak, *Phys. Rev. B*, 1996, **54**, 8252-8260.

32. A. Vanossi, N. Manini, M. Urbakh, S. Zapperi and E. Tosatti, *Rev. Mod. Phys.*, 2013, **85**, 529-552.

33. S. J. Lombardo and A. T. Bell, *Surf. Sci. Rep.*, 1991, **13**, 3-72.

34. H. Ö. Pamuk and T. Halicioğlu, *physica status solidi (a)*, 1976, **37**, 695-699.

35. R. Mahaffy, R. Bhatia and B. J. Garrison, *J. Phys. Chem. B*, 1997, **101**, 771-773.

36. S. Arcidiacono, J. H. Walther, D. Poulikakos, D. Passerone and P. Koumoutsakos, *Phys. Rev. Lett.*, 2005, **94**, 105502.

37. V. Zaloj, M. Urbakh and J. Klafter, *Phys. Rev. Lett.*, 1999, **82**, 4823-4826.

38. O. M. Braun and M. Peyrard, *Phys. Rev. E*, 2001, **63**, 046110.

39. W. Ouyang, M. Ma, Q. Zheng and M. Urbakh, *Nano Lett.*, 2016, **16**, 1878-1883.